Supplementary Information

Self-assembled micellar nanocomplexes comprising green tea catechin derivatives and protein drugs for cancer therapy

Joo Eun Chung[†]*, Susi Tan[†], Shu Jun Gao, Nunnarpas Yongvongsoontorn, Soon Hee Kim, Jeong Heon Lee, Hak Soo Choi, Hirohisa Yano, Lang Zhuo, Motoichi Kurisawa* and Jackie Y. Ying

[†]These authors contributed equally to this work

*e-mail: jechung@ibn.a-star.edu.sg; mkurisawa@ibn.a-star.edu.sg

1. Synthesis of oligomerized EGCG (OEGCG)

OEGCG was synthesized by the coupling of EGCGs through an ethyl (CH_3-CH) bridge in the presence of acetaldehyde (Fig. S1a). Studies have shown that the condensation of (+)-catechin or (-)-epicatechin in the presence of acetaldehyde gave the condensed A rings of catechins through the CH_3-CH bridges linked at C6-C6, C8-C8 and C6-C8 (R and S) bonds (Saucier, C., Guerra, C., Pianet, I., Laguerre, M. & Glories, Y. (+)-Catechin-acetaldehyde condensation products in relation to wine-ageing. *Phytochemistry* **46**, 229-234 (1997)).

To synthesize OEGCG, EGCG (Kurita Ltd., Japan) (1 g) was dissolved in a mixture of acetic acid, water and dimethyl sulfoxide (DMSO). The reaction was initiated with the addition of acetaldehyde (7.2 ml), and was conducted at 20 °C (pH 2) under a nitrogen atmosphere for 48 h. The resulting products were dialyzed (molecular weight cut-off (MWCO) = 2000) and

lyophilized to give OEGCG.

2. NMR analysis of OEGCG (DMSO-d_6):

^{1}H and ^{13}C NMR analysis of the product revealed the disappearance of H6 and H8, as well as the creation of the methyl and methine carbons of the CH_3-CH bridge, respectively, demonstrating the condensation of EGCG linked through a CH_3-CH bridge at the C6 and C8 position of the A ring.

^{1}H NMR: δ 1.3-1.7 (CHC*H*$_3$), 2.8 (H4β of C ring), 3.1 (H4α of C ring), 5.0 (H2 of C ring), 5.4 (H3 of C ring), 6.5 (H2" and 6" of D ring), 6.8 (H2' and 6' of B ring).

^{13}C NMR: δ 20.7 (CH*C*H$_3$), 26.5 (*C*HCH$_3$), 30.7 (C4 of C ring), 67.7 (C3 of C ring), 76.7 (C2 of C ring), 90.2-95.7 (C6 and 8 of A ring), 100.5 (C4a), 106.3 (C2' and 6' of B ring), 109.6 (C2" and 6" of D ring), 119.3 (C1" of D ring), 128.5 (C4' of B ring), 132.8 (C1' of B ring), 138.7 (C4" of D ring), 145.4-145.8 (C3' and 5' of B ring and C3" and 5" of D ring), 151.4-152.1 (C5 and 7 of A ring and C8a), 165.3 (*C*OO).

3. Mass spectra of OEGCG

Matrix-assisted laser desorption ionization time-of-flight mass spectrometry (MALDI-TOF MS) detected the presence of hexamer with a series of peaks separated by the regular incremental mass of an EGCG unit linked by the CH_3-CH bridge (m/z = 485 of EGCG-CHCH$_3$ fragment and m/z = 511 of CH$_3$CH-EGCG-CHCH$_3$ fragment) (Fig. S2a). MALDI-TOF/TOF analysis further proved that the parent peaks were comprised of the same fragments of EGCG molecule linked with CH_3-CH (m/z = 485 and m/z = 511) (Fig. S2b).

4. Synthesis of poly(ethylene glycol)-EGCG (PEG-EGCG)

PEG-EGCG was synthesized by conjugation between a terminal aldehyde group of PEG-CHO and the A ring of EGCG using the same reaction for OEGCG synthesis (Fig. S1b). The aldehyde-terminated PEG (PEG-CHO, Mw 5000, NOF Co., Japan) (0.35 g) and EGCG (0.65 g) were separately dissolved in a mixture of acetic acid, water and DMSO. The reaction was initiated with the dropwise addition of the PEG-CHO solution, and was conducted at 20 °C (pH 2) under a nitrogen atmosphere for 48 h. The resulting products were dialyzed (MWCO = 3500) and lyophilized to give PEG-EGCG.

5. NMR analysis of PEG-EGCG (DMSO-d_6)

The linkage between PEG and EGCG was detected by ^{13}C NMR analysis.

^{1}H NMR: δ 2.7 (H4β of C ring), 2.9 (H4α of C ring), 3.4-3.7 (CH_3O and CH_2CH_2O of PEG), 5.0 (H2 of C ring), 5.4 (H3 of C ring), 5.8-5.9 (H6 and 8 of A ring), 6.4 (H2" and 6" of D ring), 6.8 (H2' and 6' of B ring).

^{13}C NMR: δ 26.4 (*C*H of PEG linked to EGCG), 30.6 (C4 of C ring), 57.9 (*C*H_3O of PEG), 69.7-71.2 (*C*H_2*C*H_2O of PEG), 76.3 (C3 of C ring), 86.3 (C2 of C ring), 94.2-95.3 (C6 and 8 of A ring), 97.4 (C4a), 105.6 (C2' and 6' of B ring), 108.7 (C2" and 6" of D ring), 119.3 (C1" of D ring), 128.5 (C4' of B ring), 132.2 (C1' of B ring), 138.4 (C4" of D ring), 145.3-145.5 (C3' and 5' of B ring and C3" and 5" of D ring), 153.8-156.4 (C5 and 7 of A ring and C8a), 165.2 (*C*OO).

6. Mass spectra of PEG-EGCG

Electrospray ionization time-of-flight mass spectrometry (ESI-TOF MS) was conducted

on PEG (Fig. S3a) and PEG-EGCG (Fig. S3b). The m/z difference between two clusters of peaks was observed as a PEG repeating unit of 44 for both PEG and PEG-EGCG, taking into account of a charge of +5 calculated from 0.2 m/z difference between each peak (i.e. (1037.26 - 1028.43) × 5 = 44.15). However, the peaks of PEG-EGCG shifted higher with molecular weight of two EGCG (i.e. (1211.09 - 1028.65) × 5 = 912.36), as compared to those of PEG, demonstrating that the product had two molecules of EGCG bound to an end of the PEG chain.

7. Selective cancer cell growth inhibitory effect of OEGCG and PEG-EGCG

Cytotoxicities of EGCG derivatives and intact EGCG were examined on a human normal mammary epithelial cells (HMECs, Cambrex, USA). Cells were plated (1×10^4 cells in mammary epithelial growth medium/well) in quintuplicate and octuplicate for samples and controls, respectively, in 96-well microplates, and allowed to adhere overnight. After the cells were treated with different concentrations of EGCG, OEGCG and PEG-EGCG for 3 days, the cell viability was estimated using Alamar Blue. PEG-EGCG did not affect cell growth in the range of concentrations tested. Like EGCG, OEGCG showed a low cytotoxicity (Fig. S4a).

Cancer cell growth inhibitory effect of EGCG derivatives was examined on BT-474 (HER2-overexpressing human breast cancer cell line). Cells were plated (1×10^4 cells in RPMI 1640/well), and treated in the same way as mentioned above. OEGCG and PEG-EGCG both inhibited cancer cell growth in a concentration-dependent manner (Fig. S4b).

8. ζ Potential of Herceptin-loaded MNC

ζ potential was analysed at each step of these two-step sequential self-assemblies (Fig. S6). ζ potential was measured using a zeta potential analyser (Brookhaven Instruments Co.). The

surface charge of the Herceptin/OEGCG complexes was observed to be positive. After adding the required amount of PEG-EGCG to the Herceptin/OEGCG complexes, the surface charge of the resulting complex decreased to a value close to that of PEG. This finding confirmed that the MNC was constructed with a PEG outer shell that surrounded the Herceptin/OEGCG core.

9. Protection from proteolysis

To investigate the protection of protein by this system, the MNC loaded with a fluorescence-labeled protein (fluorescein isothiocyanate-bovine serum albumin (FITC-BSA) was subjected to a protease (proteinase K, 0.05 mg ml^{-1}), and the fluorescence intensity increase due to protein degradation was monitored (Fig. S9). A fluorescence spectrophotometer was employed for this study (Hitachi, Japan, λ_{ex} = 490 nm and λ_{em} = 530 nm). The fluorescence intensity of free FITC-BSA increased significantly with time, indicating the progressive protein degradation by proteinase K. In contrast, the fluorescence intensity of FITC-BSA loaded in the MNC increased very slowly, indicating that the protein was safely protected from proteolysis by this MNC system.

10. *In vitro* synergism study of Herceptin-MNC

The quantitative analysis of the combined therapeutic effects of Herceptin and the carrier components in the Herceptin-MNC system was performed using the combination index (CI) theorem of Chou-Talalay, which offers quantitative definition of the additive effect (CI = 1), synergism (CI < 1), and antagonism (CI > 1) in drug combinations (Chou, T.-C., *et al. Adv Enzyme Regul* **22**, 27-55 (1984)). The Chou-Talalay method has been widely used for dose effect analysis quantifying synergism/antagonism in drug combination (Chou, T.-C., *et al. J Natl*

Cancer I **86**, 1517-1524 (1994)). The general equation for the combination index $^{n}(CI)_x$ for *n* drugs at *x*% inhibition is described as,

$$^{n}(CI)_x = \sum_{j=1}^{n} \frac{(D)_j}{(D_x)_j}$$

where $(D)_j$ is the concentrations of *n* drugs used in combination to achieve *x*% drug effect, and $(D_x)_j$ is the concentrations of each drug alone to achieve the same effect. Based on this theory, the computer software CalcuSyn was developed for automated data analysis (Chou, T.-C., *et al. J Natl Cancer I* **86**, 1517-1524 (1994)).

Since Herceptin-MNC (Herceptin = 0.5 mg ml^{-1}, OEGCG = 0.024 mg ml^{-1}, PEG-EGCG = 0.26 mg ml^{-1}) gave an inhibition effect of 0.52 on BT-474 cells (Fig. 4a), CI of three therapeutic components (Herceptin/OEGCG/PEG-EGCG) in the Herceptin-MNC was calculated by the following equation using the CalcuSyn software.

$$CI = \frac{(D)_{Herceptin}}{(D_{52})_{Herceptin}} + \frac{(D)_{OEGCG}}{(D_{52})_{OEGCG}} + \frac{(D)_{PEG-EGCG}}{(D_{52})_{PEG-EGCG}}$$

where $(D)_{Herceptin}$, $(D)_{OEGCG}$ and $(D)_{PEG\text{-}EGCG}$ are the concentrations of Herceptin, OEGCG and PEG-EGCG used in combination to achieve 52% drug effect. $(D_{52})_{Herceptin}$, $(D_{52})_{OEGCG}$ and $(D_{52})_{PEG\text{-}EGCG}$ are the concentrations for Herceptin, OEGCG and PEG-EGCG, respectively, to achieve the same effect independently. Each value was computed from the dose effect curve that was generated by the CalcuSyn. The resulting CI of Herceptin-MNC was 0.93 (CI < 1), indicating the synergistic therapeutic effect between Herceptin and the carrier components.

11. Toxicity of Herceptin and Herceptin-MNC

The change of each organ in mice was determined microscopically 35 days after the

administration of Herceptin (2.5 mg kg^{-1}) or Herceptin-MNC in an equivalent amount to Herceptin (Table S1).

12. Anticancer effects of IFN-MNC *in vitro* and *in vivo*

HAK-1B (human liver cancer cell line) was kindly provided from Prof. Hirohisa Yano (Kurume University, Japan). HAK-1B was cultured in DMEM with 5% FBS and 100 units ml^{-1} of penicillin and streptomycin. Inhibitory effect of IFN-MNC in HAK-1B proliferation was analysed in the same way mentioned in the main text with following samples: IFN (0.020 mg ml^{-1}), IFN-MNC (IFN/OEGCG/PEG-EGCG = 0.020/0.0049/0.78 mg ml^{-1}), BSA-MNC (with the equivalents), the mixture of BSA-MNC and IFN (with the equivalents), BSA (with the equivalent), OEGCG (with the equivalent), and PEG-EGCG (with the equivalent).

To analyse anticancer effect of IFN-MNC in tumour-xenografted nude mice, CrTac:NCr-Foxn1nu female mice were inoculated s.c. with 1×10^7 HAK-1B cells suspended in 200 μl of PBS at the right flank. Once the tumours reached a volume of 360 mm^3, 8-9 mice/group were randomly allocated for different treatment. Treatment, measurement and analysis were performed in the same way mentioned in the main text with following samples: PBS (vehicle control), free IFN, BSA-MNC, a sequential administration of BSA-MNC and IFN, and IFN-MNC in the same formulations as those employed in the *in vitro* experiments.

13. Bioconjugation of NIR fluorophores

Heptamethine near-infrared (NIR) fluorophore ZW800-1 was synthesized as previously reported (Choi, H.S., *et al. Angew Chem Int Ed Engl* **50**, 6258-6263 (2011)). Herceptin-ZW800-1 (HER-ZW) or interferon-ZW800-1 (IFN-ZW) was prepared in 0.1 M sodium phosphate buffer

(pH 8) by adding 5 equivalents of ZW800-1 to the Herceptin or IFN solution. To purify the reaction mixture, gel-filtration chromatography (GFC) was performed using Bio-Scale Mini Bio-Gel P-6 Desalting columns (Bio-Rad) with 0.05 M phosphate buffer as an eluent. The conjugated protein fractions were collected and concentrated using spin columns (Vivaspin 500, MWCO = 50,000). The conjugation ratio was estimated from the ratio of extinction coefficients between ZW800-1 ($\varepsilon_{772\ nm}$ = 249,000 M^{-1} cm^{-1}) and Herceptin ($\varepsilon_{280\ nm}$ = 225,000 M^{-1} cm^{-1}) or IFN ($\varepsilon_{280\ nm}$ = 14,500 M^{-1} cm^{-1}) with correction for the 5% measured absorbance at 280 nm due to ZW800-1. Labeling ratio was ~ 1 for HER-ZW and ~ 0.5 for IFN-ZW conjugates, which was calculated by the following formula, $(Abs_{772\ nm}/\varepsilon_{772\ nm})/[(Abs_{280\ nm} - 0.05Abs_{772\ nm})/\varepsilon_{280\ nm}]$. Absorbance and fluorescence emission spectra of fluorophore-conjugated proteins and protein-MNCs are shown in Fig. S14 and S16, respectively.

14. Biodistribution and pharmacokinetics

For tumour-bearing animals, the accumulation ratio of the tumour to normal organ/tissue was measured using a region of interest (ROI) over the tumour for fluorescence (FL) and a ROI over liver, kidney, spleen or skin for background (BG) after resection (Fig. 4e and Fig. S17). The blood half-life of proteins and protein-MNCs was compared in Fig. S15 and S18. At least five animals were analysed. Statistical analysis was performed using a one-way ANOVA, followed by Tukey's multiple comparisons test. The curve fitting was performed using Prism version 4.0a software (GraphPad, San Diego, CA).

SUPPLEMENTARY TABLE

Supplementary Table 1

Table S1. Pathological findings after administration of Herceptin or Herceptin-MNC

Organs	Herceptin	Herceptin-MNC
Brain	N	N
Lung	N	N
Heart	N	N
Kidneys	N	N
Liver	N	N
Gallbladder	N	N
Spleen	N	N

N: Normal

SUPPLEMENTARY FIGURES

Supplementary Fig. 1

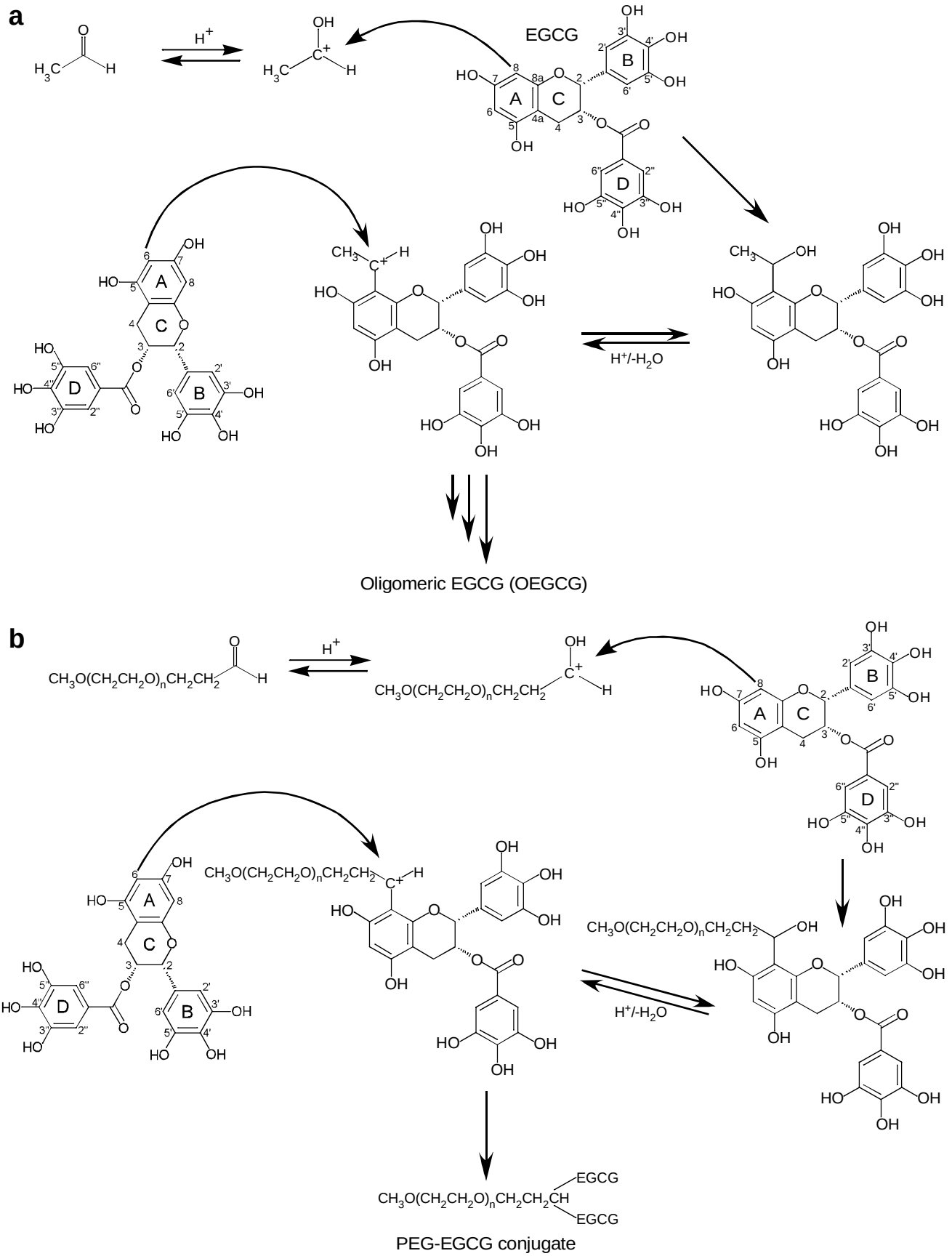

Fig. S1 Synthesis of carrier components. Synthesis of **a,** OEGCG and **b,** PEG-EGCG.

Supplementary Fig. 2

a.

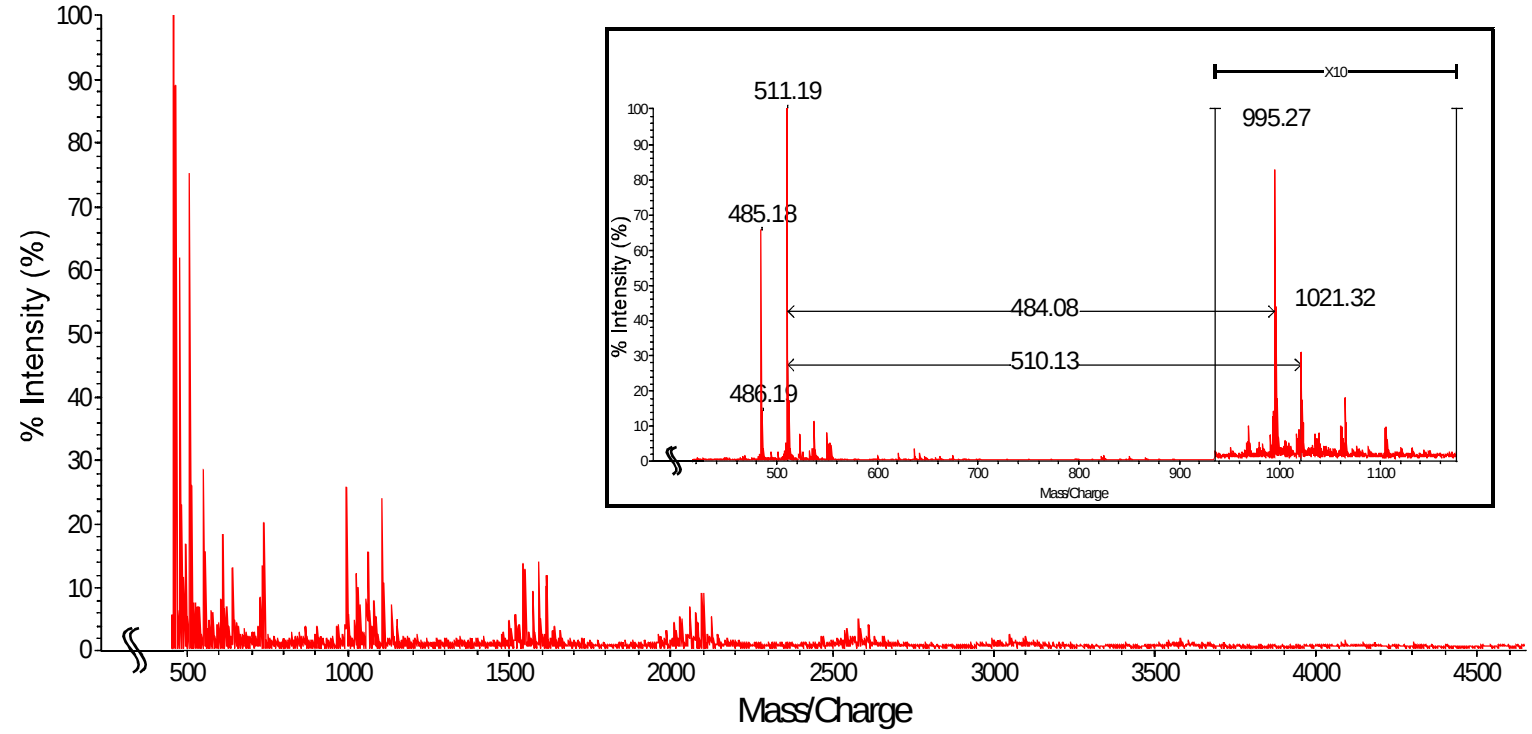

b.

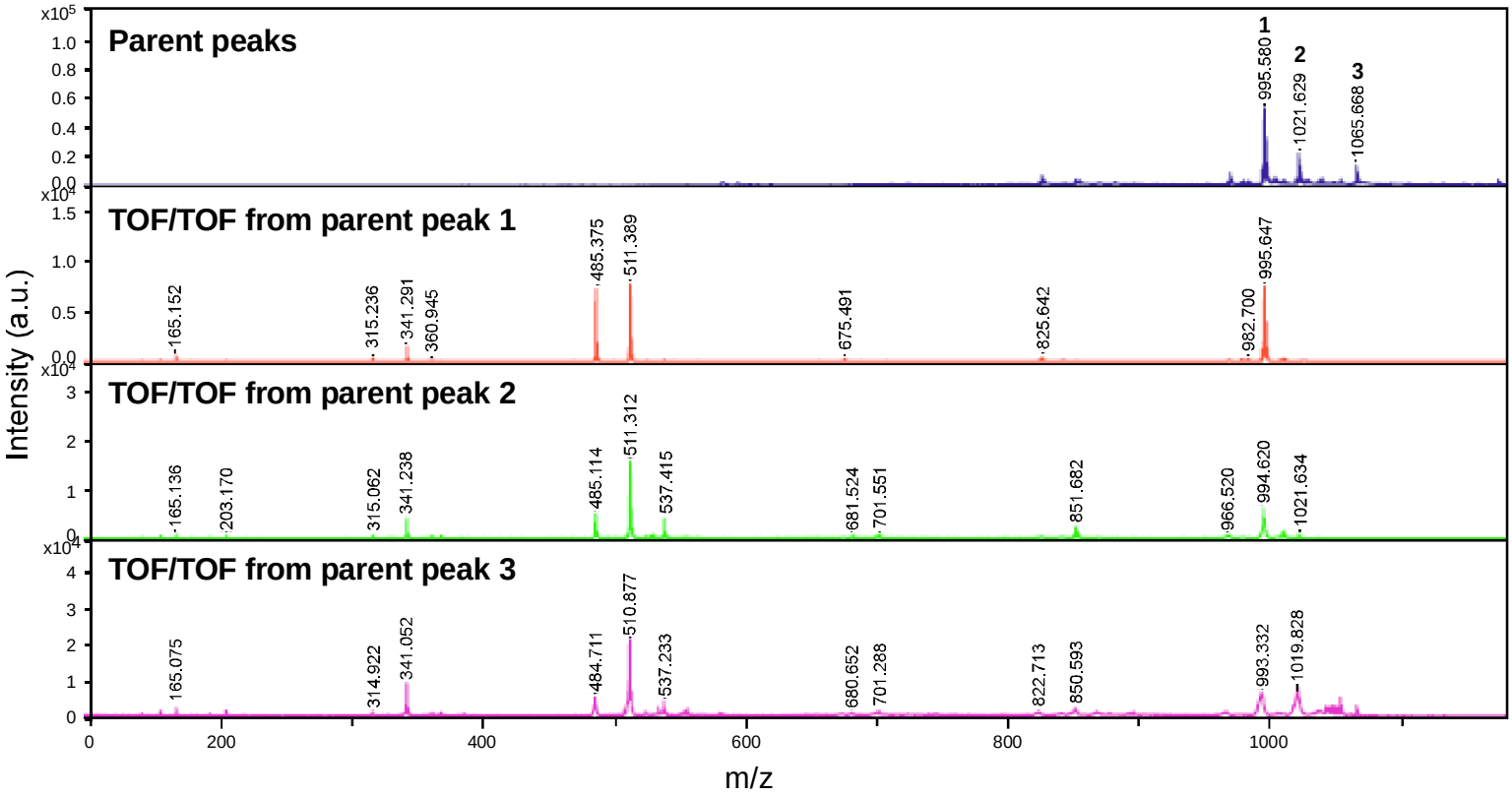

Fig. S2 Mass spectra of OEGCG. a, MALDI-TOF mass spectrum of OEGCG. **b,** MALDI-TOF/TOF mass spectrum of OEGCG.

Supplementary Fig. 3

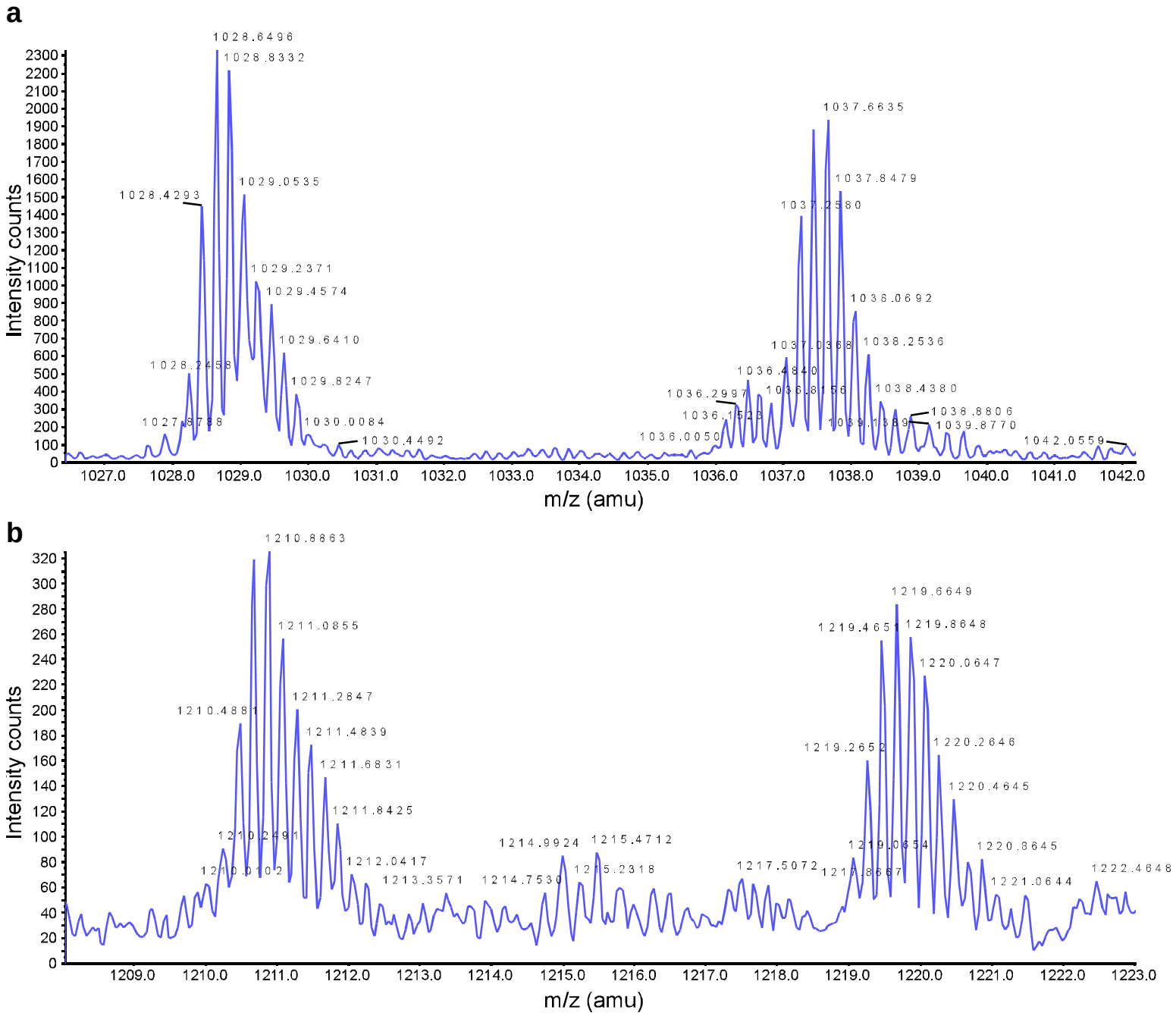

Fig S3 ESI-TOF mass spectrum of PEG-EGCG. Zoom-in spectra of +5 charged fragments of **a,** PEG and **b,** PEG-EGCG.

Supplementary Fig. 4

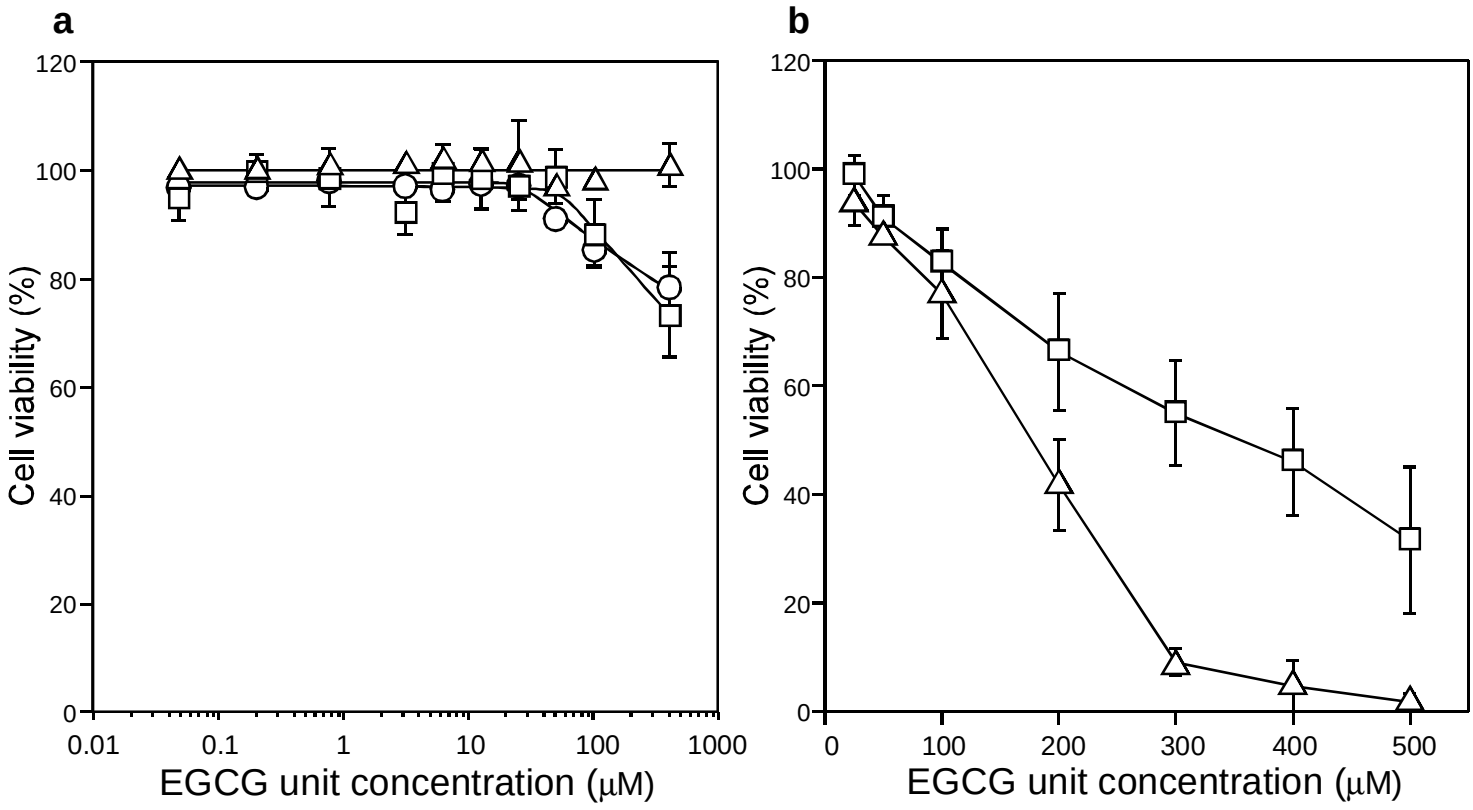

Fig. S4 Cell growth inhibitory effect. a, HMECs (human normal mammary epithelial cells) and **b,** BT-474 (HER2-overexpressing human breast cancer cell line) treated with EGCG (white circles), OEGCG (white squares) and PEG-EGCG (white triangles). The data points represent mean values and the bars represent s.d. (n = 5).

Supplementary Fig. 5

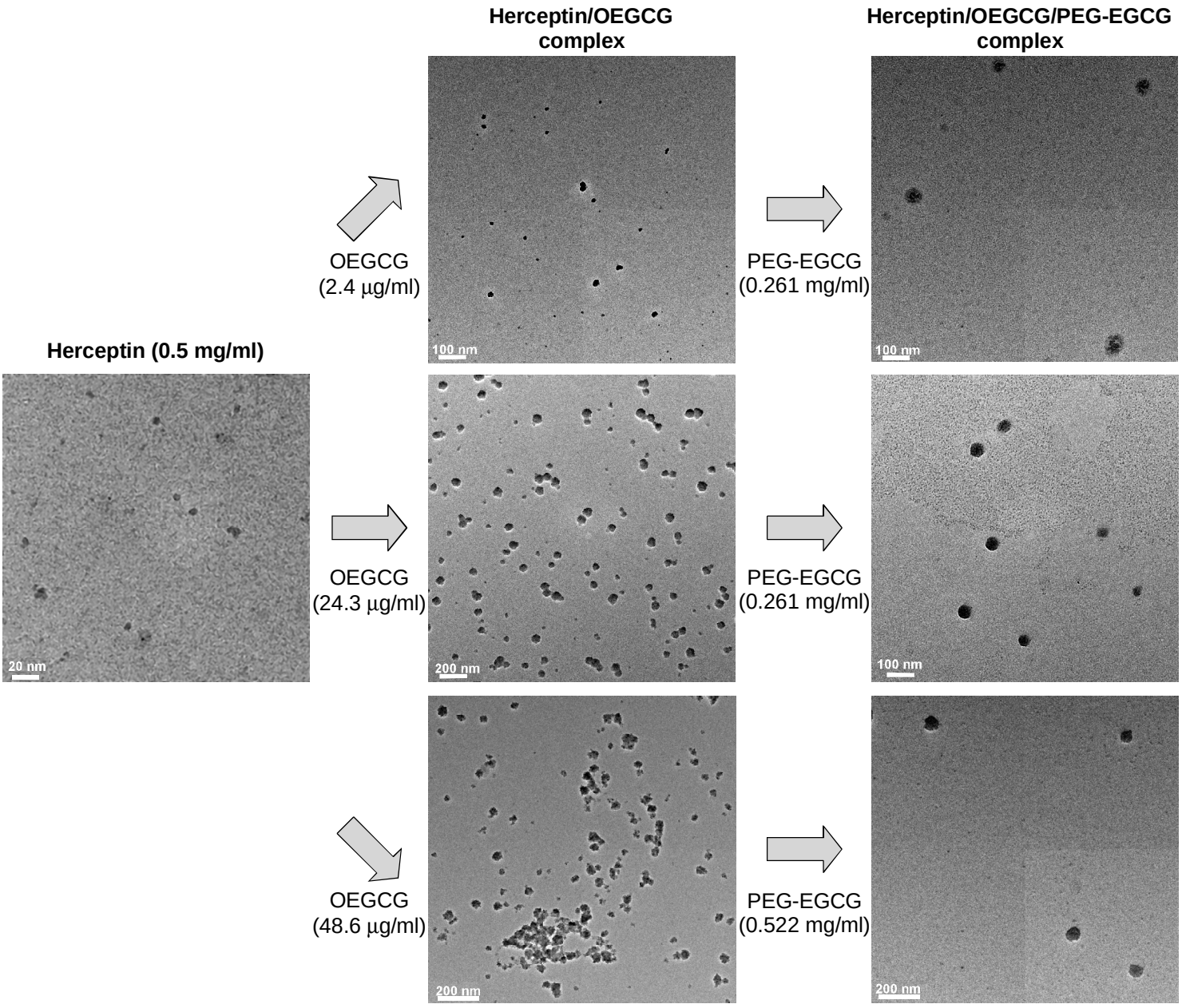

Fig. S5 TEM images of complexes observed at each step of self-assembly, when the OEGCG concentration was varied.

Supplementary Fig. 6

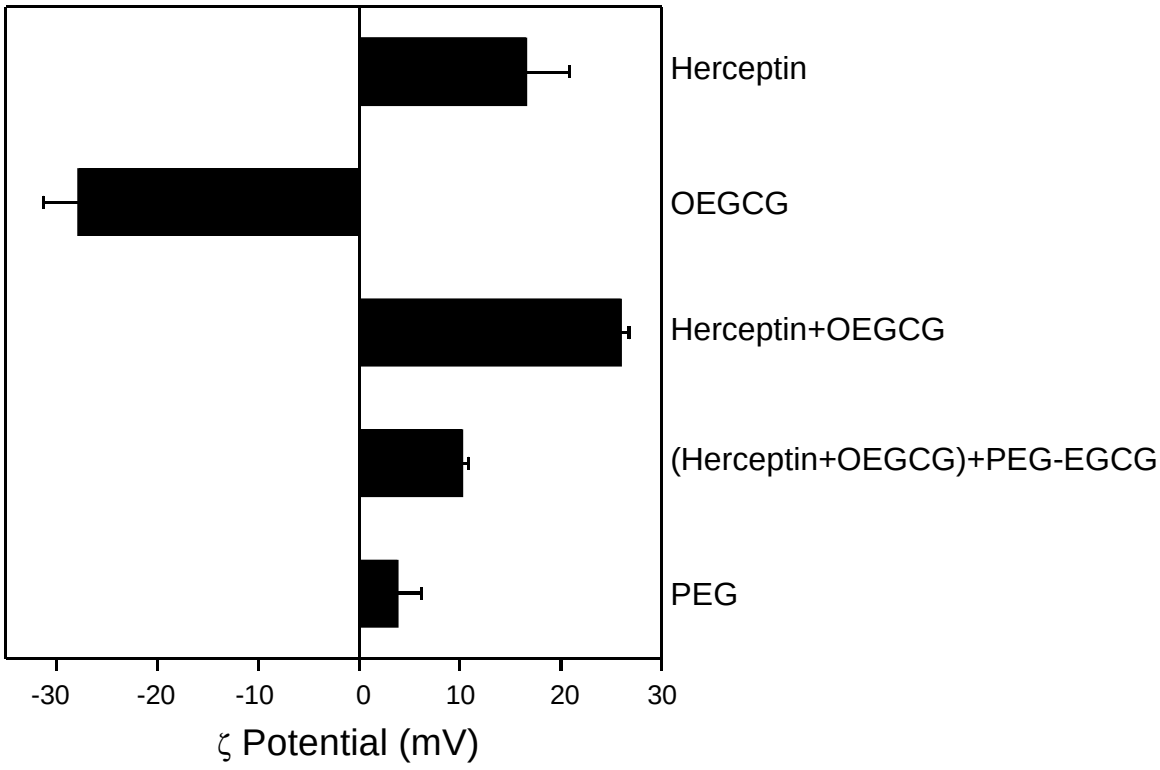

Fig. S6 Surface charge of the complexes observed at each assembly step. The results are reported as mean values and the bars represent s.d. (n = 5).

Supplementary Fig. 7

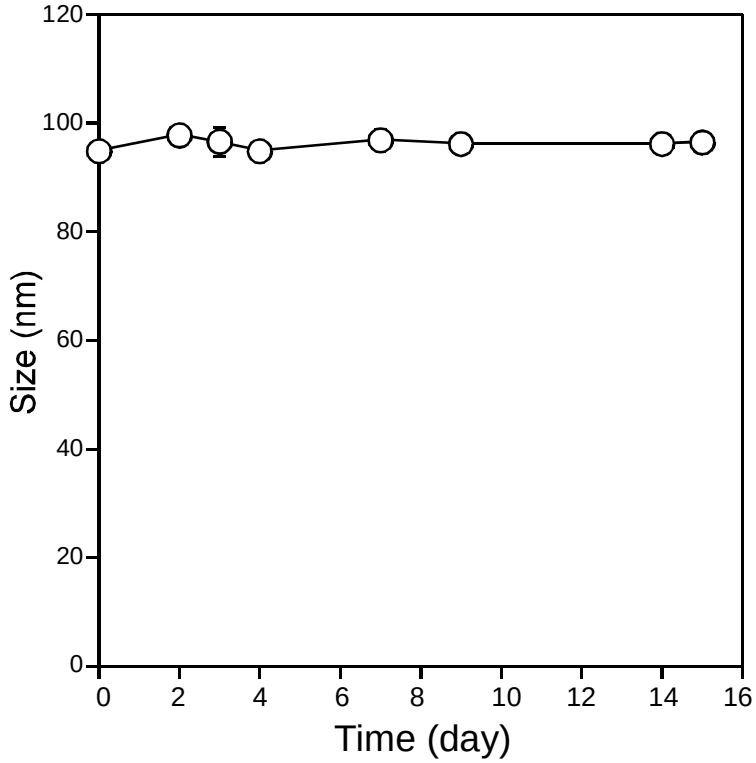

Fig. S7 Integrity of the MNC in the presence of serum at 37°C. The data points represent mean values and the bars represent s.d. (n = 3).

Supplementary Fig. 8

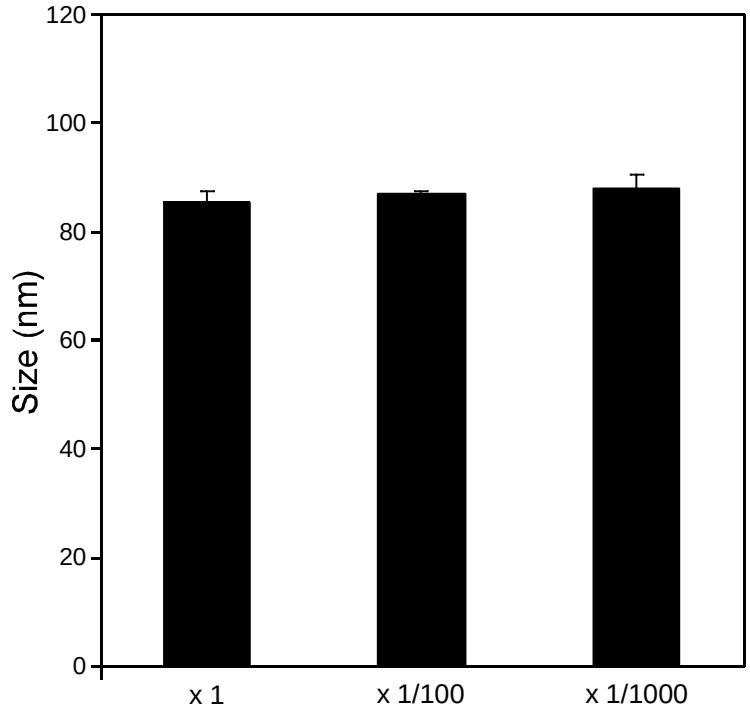

Fig. S8 Integrity of the MNC in dilution. The results are reported as mean values and the bars represent s.d. (n = 3).

Supplementary Fig. 9

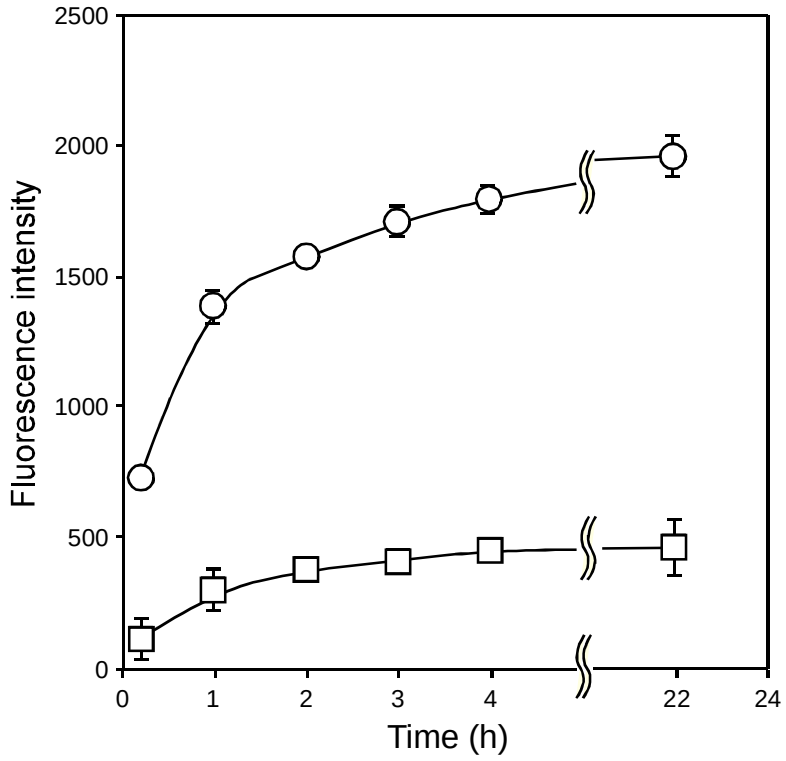

Fig. S9 Protection against proteolysis by complexation. Free FITC-BSA (white circles) and FITC-BSA loaded MNC (white squares) in the presence of proteinase K. The data points represent mean values and the bars represent s.d. (n = 3).

Supplementary Fig. 10

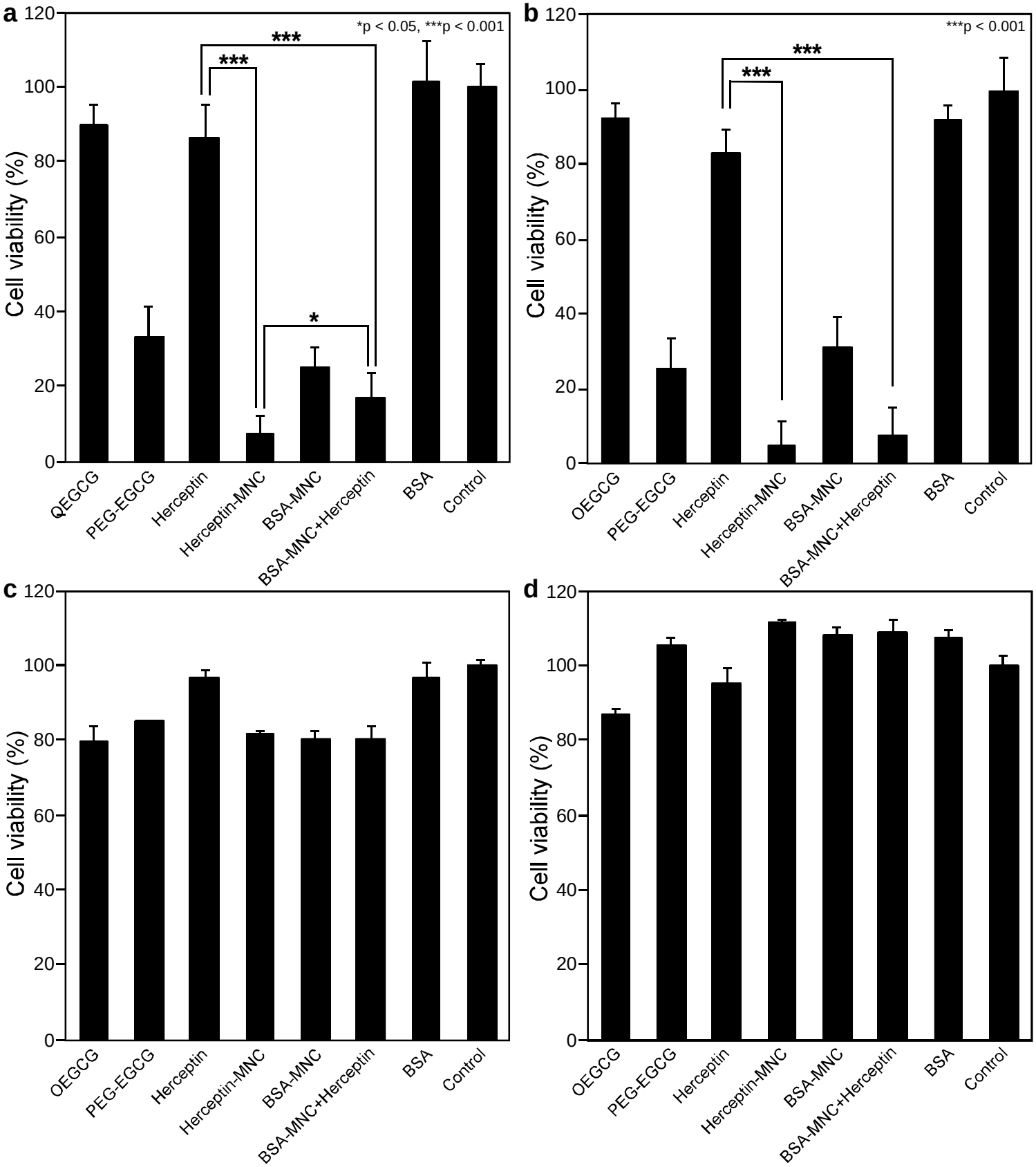

Fig. S10 Cell growth inhibitory effect. Effect on **a,** SKBR-3 (human breast cancer cells), **b,** SKOV-3 (human ovarian cancer cells), **c,** MCF-10A (human normal mammary epithelial cells) and **d,** HMEC (human normal mammary epithelial cells) by control (untreated), Herceptin (0.5 mg ml^{-1}), Herceptin-MNC (Herceptin/OEGCG/PEG-EGCG = 0.5/0.024/0.26 mg ml^{-1}), BSA-MNC (drug-free carrier, with the equivalents), a mixture of BSA-MNC and Herceptin (with the equivalents), BSA (with the equivalent), OEGCG and PEG-EGCG (carrier components, with the equivalents), n = 5 (mean ± s.d.). *p < 0.05, ***p < 0.001.

Supplementary Fig. 11

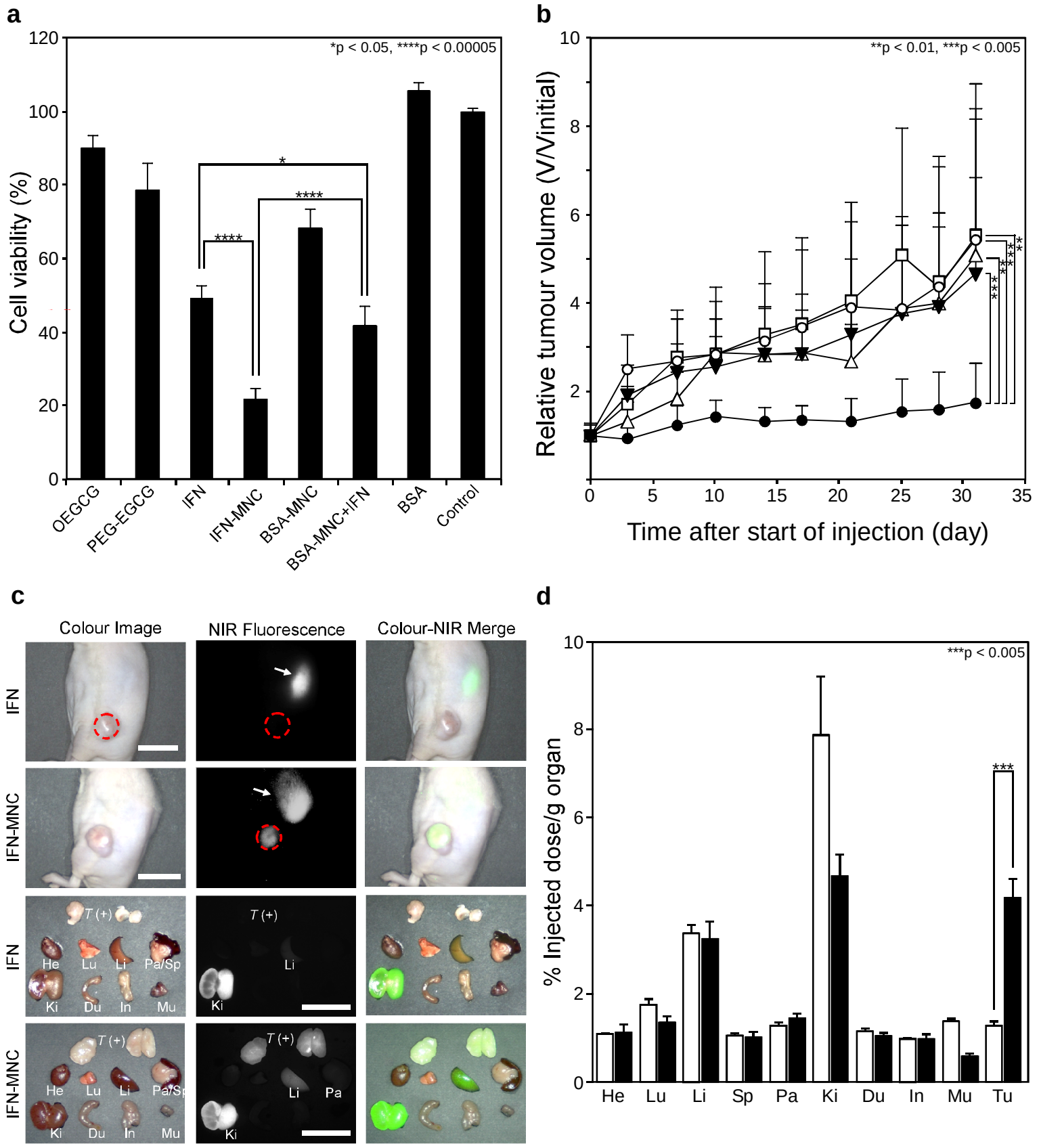

Fig. S11 The anticancer effect and biodistribution of the IFN-MNC. a, HAK-1B (human liver cancer cell line) growth inhibitory effects by control (untreated), IFN (0.020 mg ml^{-1}), IFN-MNC (IFN/OEGCG/PEG-EGCG = 0.020/0.0049/0.78 mg ml^{-1}), BSA-MNC (drug-free carrier, with the equivalents), a mixture of BSA-MNC and IFN (with the equivalents), BSA (with the equivalent), OEGCG and PEG-EGCG (carrier components, with the equivalents), n = 5 (mean ± s.d.). *p < 0.05, ****p < 0.00005. **b,** Anticancer effect on HAK-1B-xenografted nude mouse model. PBS (vehicle control, white circles), IFN (0.1 mg kg^{-1}, white squares), BSA-MNC (white triangles), sequential injection of BSA-MNC and IFN (black inverted triangles) and IFN-MNC (black circles) in the same formulations used in Fig. S11a, n = 8-9 (mean ± s.d.). **p < 0.01, ***p < 0.005. **c,** Real-time intraoperative tumour detection and biodistribution in major organ/tissue resected using NIR fluorescence. Shown are representative (n = 5) images of colour video (left), NIR fluorescence (middle), and a pseudocoloured merge of the two (right) at 24 h post-injection. Arrows = non-specific uptake (liver, kidneys, intestine); red dotted circle = ROI; T (+), positive tumour; He, heart; Lu, lung; Li, liver; Pa, pancreas; Sp, spleen; Ki, kidneys; Du, duodenum; In, intestine; Mu, muscle. Scale bars = 1 cm. **d,** Biodistribution analysis by comparing CBR (contrast-to-background ratio) of resected organ/tissue. IFN (white bars), IFN-MNC (black bars), n = 5 (mean ± s.d.). ***p < 0.005. All NIR fluorescence images have identical exposure times and normalization.

Supplementary Fig. 12

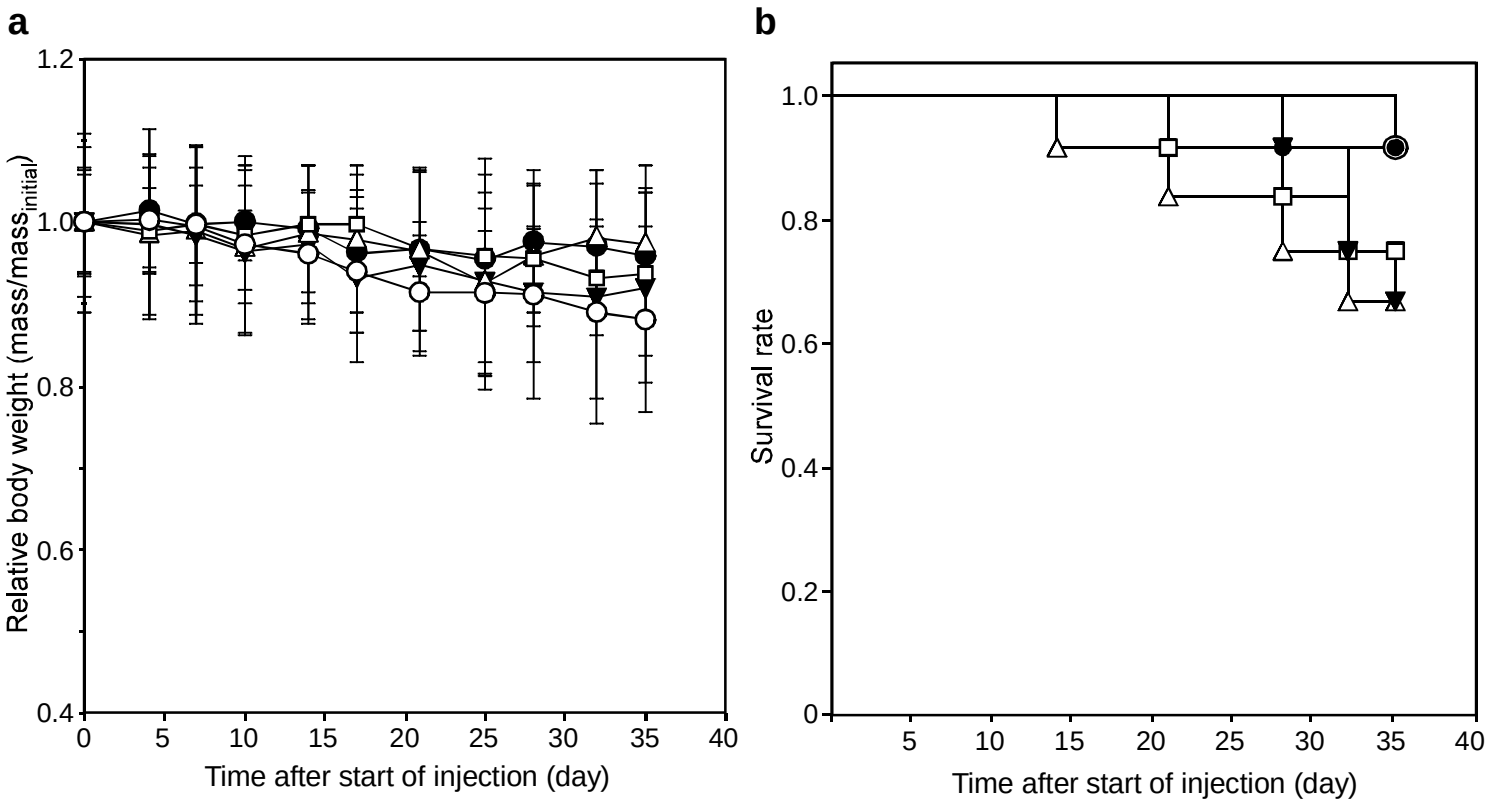

Fig. S12 The body weight and survival rate upon treatment using Herceptin-MNC. **a,** Relative body weight change of the BT-474 (human breast cancer cell line)-xenografted nude mouse during treatment, n = 12 (mean ± s.d.). Statistical analysis was performed by ANOVA. **b,** Mice survival rate during treatment. Comparisons between groups were made using a Kaplan-Meier analysis followed by the Log Rank Test. PBS (vehicle control, white circles), free Herceptin (white squares), BSA-MNC (drug-free carrier, white triangles), sequential injection of BSA-MNC and Herceptin (black inverted triangles), and Herceptin-MNC (black circles), n = 12.

Supplementary Fig. 13

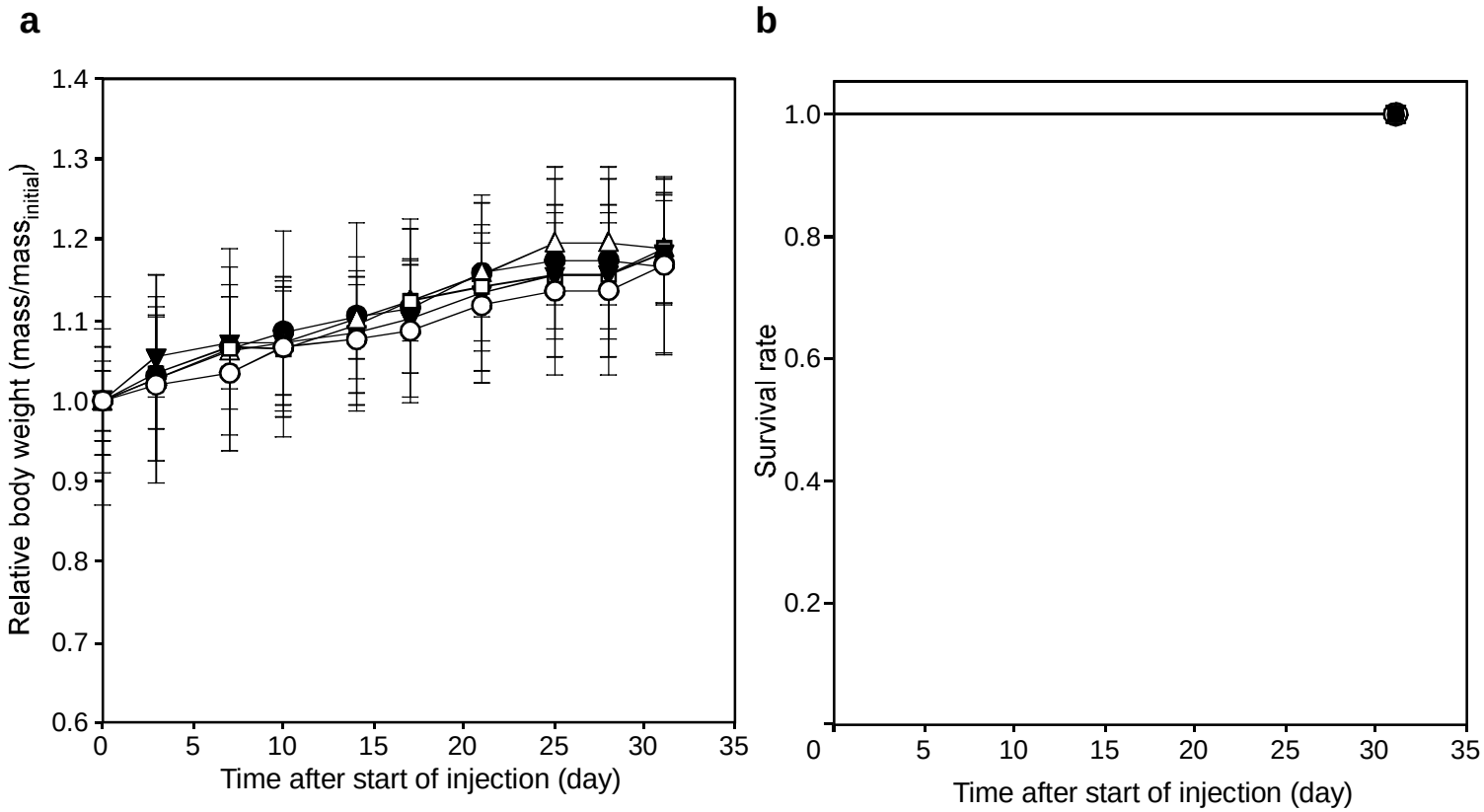

Fig. S13 The body weight and survival rate upon treatment using IFN-MNC. a, Relative body weight change of the HAK-1B (human liver cancer cell line)-xenografted nude mouse during treatment, n = 8-9 (mean ± s.d.) . **b,** Mice survival rate during treatment. Comparisons between groups were made using a Kaplan-Meier analysis followed by the Log Rank Test. PBS (vehicle control, white circles), IFN (0.1 mg kg^{-1}, white squares), BSA-MNC (white triangles), sequential injection of BSA-MNC and IFN (black inverted triangles) and IFN-MNC (black circles), n = 8-9.

Supplementary Fig. 14

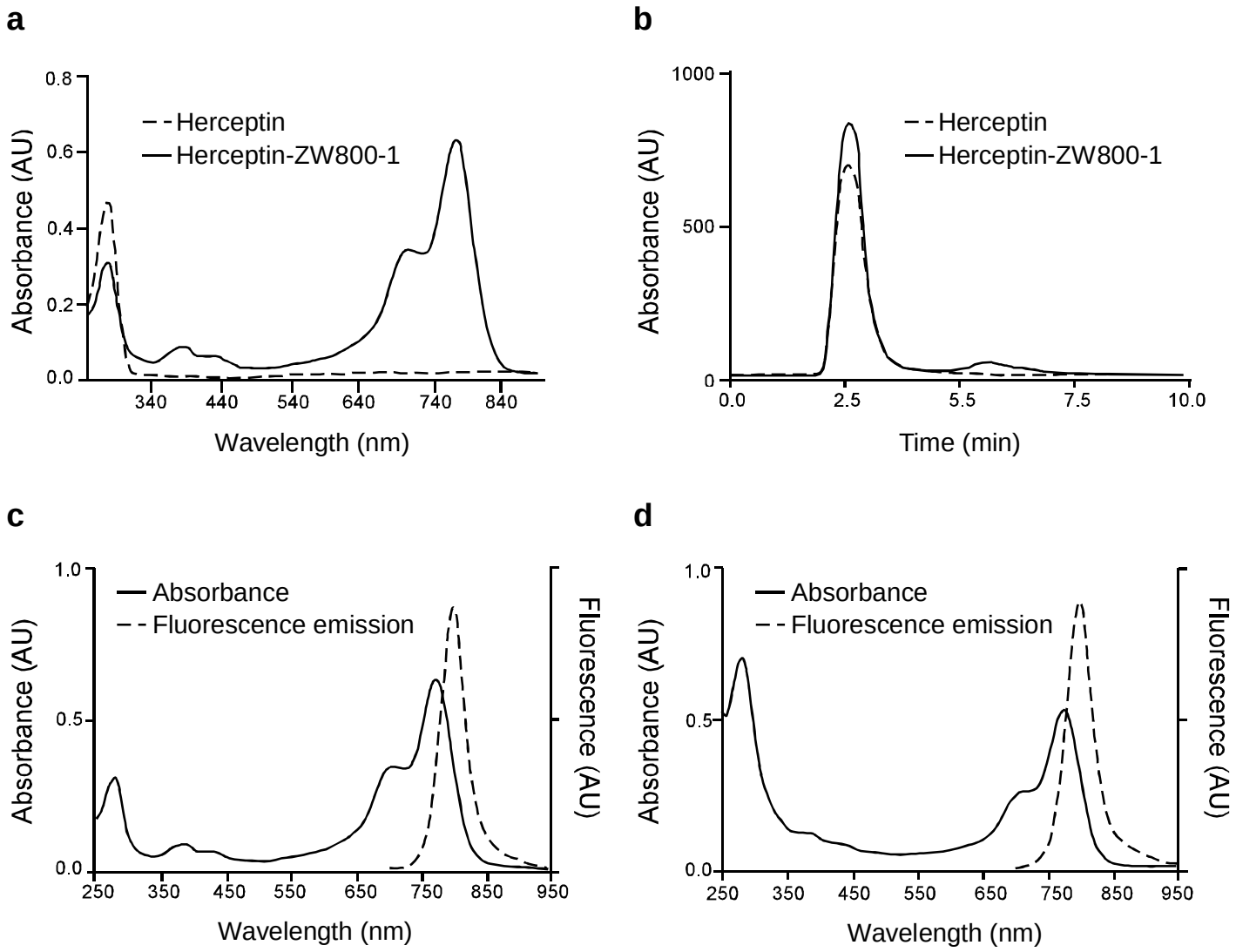

Fig. S14 Bioconjugation of NIR Fluorophores to Herceptin. a, Calculation of labeling ratio and **b,** GFC purification of Herceptin-ZW800-1. Absorbance and fluorescence emission spectra of **c,** Herceptin-ZW800-1 and **d,** Herceptin-ZW800-1-loaded micellar nanocomplex (Herceptin-ZW800-1-MNC) in PBS (pH 7.4).

Supplementary Fig. S15

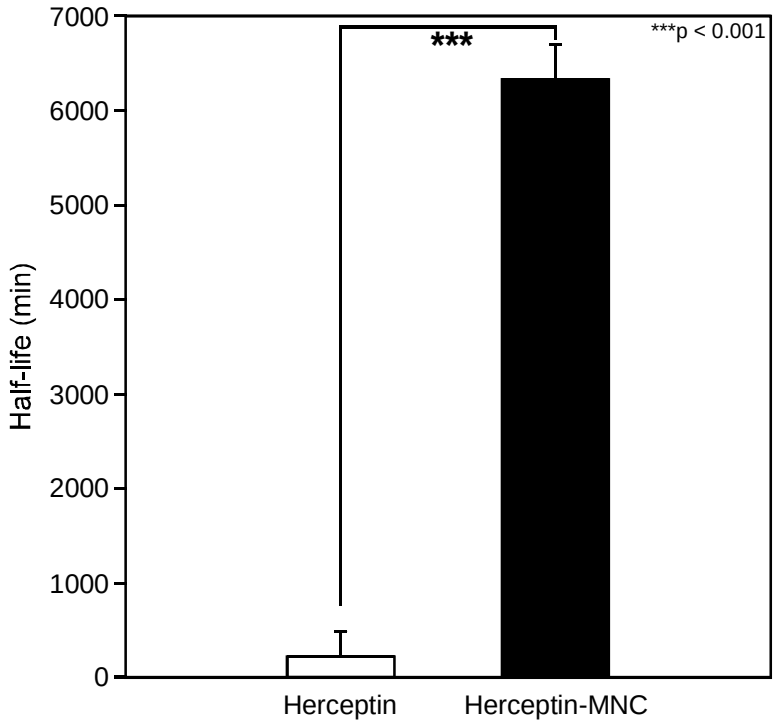

Fig. S15 Blood half-life of NIR fluorophore-labeled Herceptin and Herceptin-MNC. n = 5 (mean ± s.d.), ***p < 0.001.

Supplementary Fig. S16

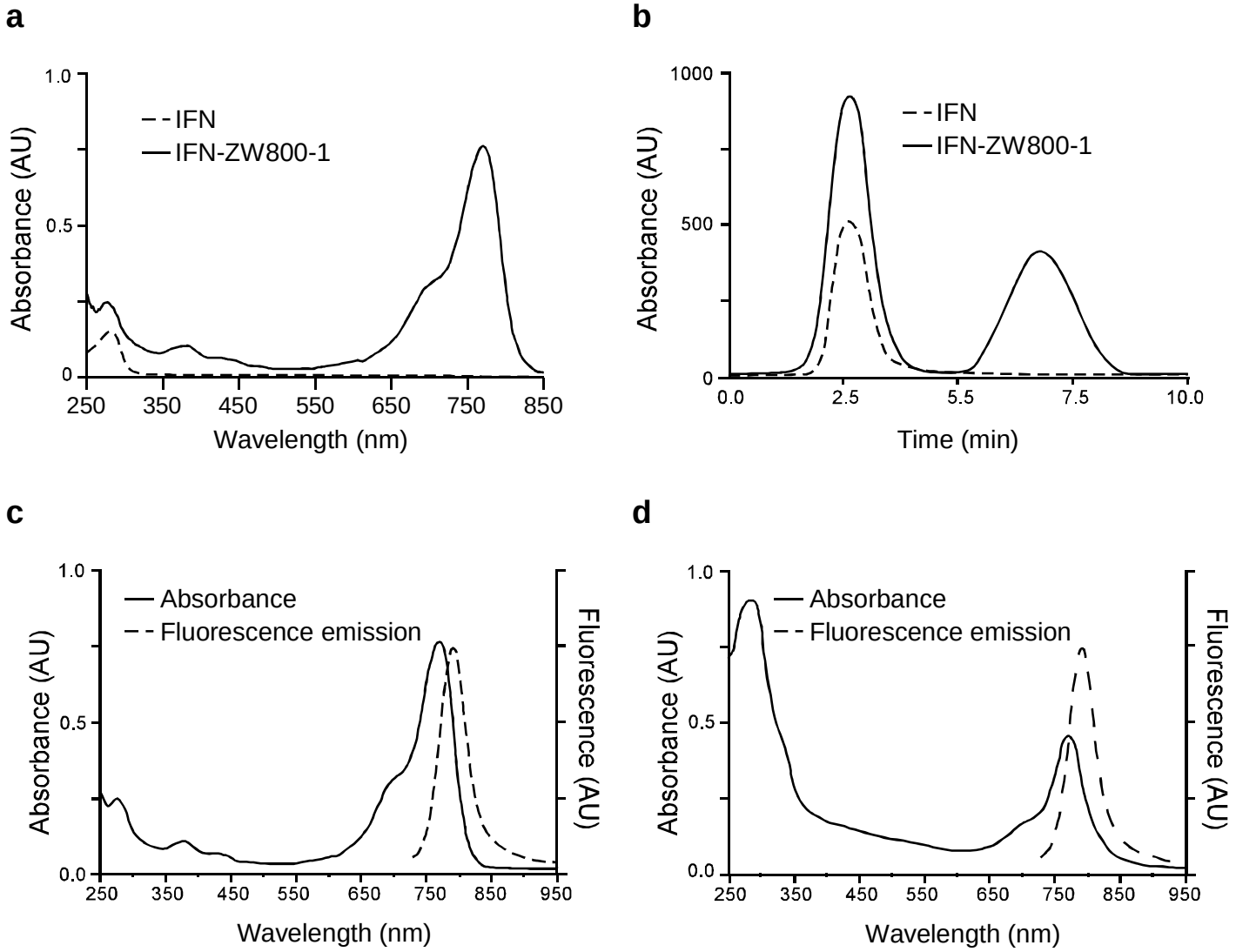

Fig. S16 Bioconjugation of NIR Fluorophores to IFN. a, Calculation of labeling ratio and **b,** GFC purification of IFN-ZW800-1. Absorbance and fluorescence emission spectra of **c,** IFN-ZW800-1 and **d,** IFN-ZW800-1-loaded micellar nanocomplex (IFN-ZW800-1-MNC) in PBS (pH 7.4).

Supplementary Fig. S17

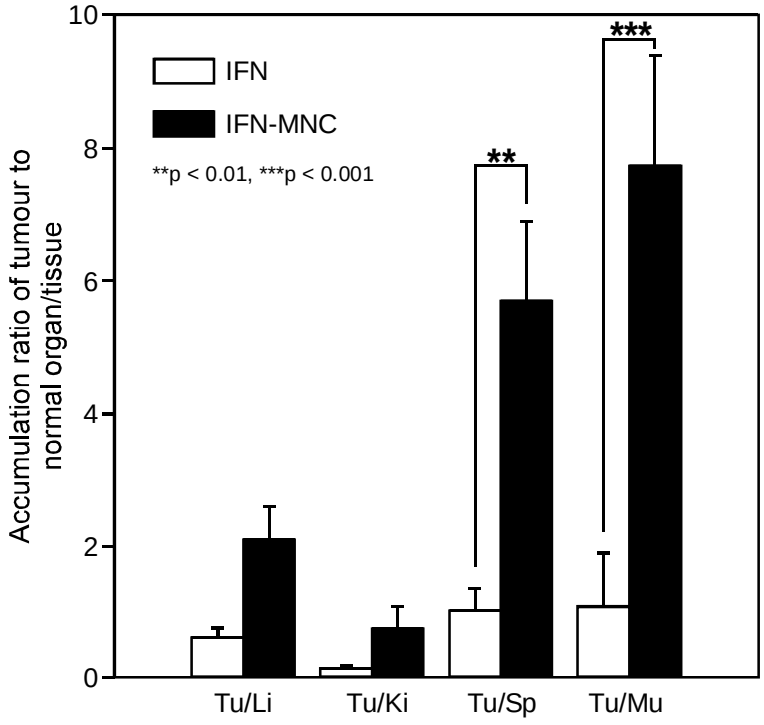

Fig. S17 Accumulation ratios of the tumour to normal organ/tissue for IFN (white bars) and IFN-MNC (black bars). n = 5 (mean ± s.d.), **p < 0.01, ***p < 0.001. Tu, tumour; Li, liver; Ki, kidney; Sp, spleen; Mu, muscle.

Supplementary Fig. S18

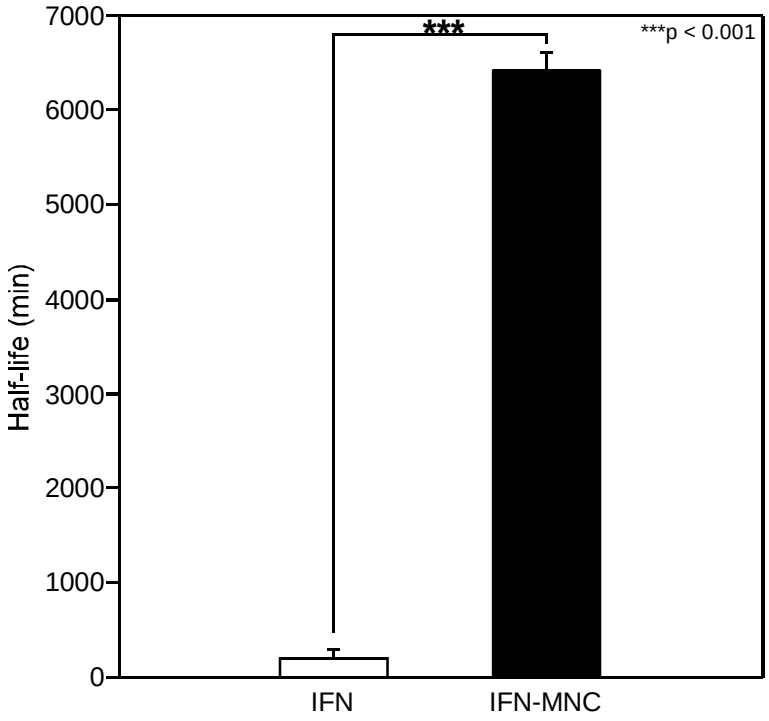

Fig. S18 Blood half-life of NIR fluorophore-labeled IFN and IFN-MNC. n = 5 (mean ± s.d.), ***p < 0.001.